A Compact and Autoclavable System for Acute Extracellular Neural Recording and Brain Pressure Monitoring for Humans

Gian Nicola Angotzi, Gytis Baranauskas, Alessandro Vato, Andrea Bonfanti, *Member, IEEE*, Guido Zambra, Emma Maggiolini, Marianna Semprini, Davide Ricci, Alberto Ansaldo, Elisa Castagnola, Tamara Ius, Miran Skrap, and Luciano Fadiga

Manuscript received July 12, 2013; revised November 18, 2013; accepted March 02, 2014. This work was supported by the Brain Machine Interface (BMI) project in the Robotics, Brain and Cognitive Sciences (RBCS) Department at "Istituto Italiano di Tecnologia," Genoa, Italy. This paper was recommended by Associate Editor S. DeWeerth.

G. N. Angotzi, A. Vato, E. Maggiolini, M. Semprini, D. Ricci, A. Ansaldo, and E. Castagnola, are with the Department of Robotics, Brain and Cognitive Sciences, Istituto Italiano di Tecnologia, 16163 Genova, Italy (e-mail: giannicola.angotzi@iit.it; emma.maggiolini@iit.it; marianna.semprini@iit.it; davide.ricci@iit.it; alberto.ansaldo@iit.it; elisa.castagnola@iit.it).

G. Baranauskas is with the Institute of Biomedical Research, Lithuanian University of Health Sciences, 73000 Kaunas, Lithuania (e-mail: Gytis.Baranauskas@lsmuni.lt).

A. Bonfanti and G. Zambra are with the Dipartimento di Elettronica e Informazione, Politecnico di Milano, 20133 Milano, Italy (e-mail: bonfanti@elet.polimi.it).

T. Ius and M. Skrap are with the Department of Neurosurgery, General Hospital, 33100 Udine, Italy.

L. Fadiga is with the Department of Robotics, Brain and Cognitive Sciences, Istituto Italiano di Tecnologia, 16163 Genova, Italy, and also with the Dipartimento di Scienze Biomediche e Terapie Avanzate, Università degli Studi di Ferrara, 44121 Ferrara, Italy.

I. Introduction

GLIOMAS make up 30% of all brain and central nervous system tumors and 80% of all malignant brain tumors [1]. In particular, low-grade gliomas are well differentiated and portend a better prognosis for the patient but within some years they become malignant [2]. Because of that, in the majority of cases low-grade gliomas are surgically removed as extensively as possible, this being correlated with a better outcome [3]–[5] . In order to spare functions of the brain regions involved by the tumor, a number of intra-operative functional mapping techniques are commonly used. Although the intra-operative electrical stimulation in awake patients is considered the gold standard for delineation of functional brain areas [6], other functional mapping methods such as motor evoked potentials [7], EEG and electrocortigraphy [8] are also used. In spite of this, large areas still remain where mapping methods are unable to provide information about their specific function and, consequently, surgical ablation of these areas might leave the patient with neurological dysfunctions [6], [9].

In this framework single and multi-unit recordings may provide a finer functional mapping by identifying brain areas that respond with changes in neuronal activity when the patient performs some actions such as speech, hand movements or is presented with visual, somatosensory or auditory stimuli. Interestingly, over the last years many groups in the world focused their research on the development of power efficient and low-noise multichannel neural recording front ends [10]–[12]. This has laid the groundwork for developing new, much more user friendly and compact multichannel recording instruments. Such equipment should be compact (to limit the intrusion into the surgical field), reliable, easily sterilizable and providing stable high-quality signals. Besides a large signal to noise ratio (SNR) of the recording front-end , which is mandatory to discriminate neural data, properly performed micro-recordings also require that the microelectrodes must be advanced along the recording track by small steps (around $10\ \mu\mathrm{m}$) to ensure the acquisition of *true* single unit activities [13].

Micromotions of the brain should finally be taken into account when performing *in-vivo* neural recordings. These minimal oscillations of the brain (around $500\ \mu\mathrm{m}$) have well-defined cardiac and respiratory components that produce a pressure variation at the brain surface having a mean amplitude

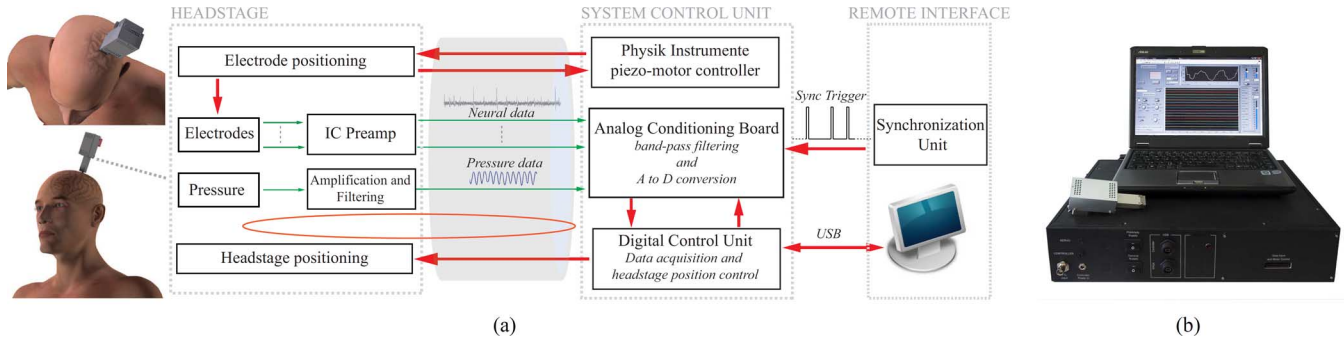

Fig. 1. (a) Basic building blocks or the proposed system. Red and green arrows portray respectively digital and analog signals. The headstage is connected to the System Control Unit with a 3 m, 26 pole unshielded ribbon cable while a USB connection allows bidirectional communication between the System Control Unit and the Graphical User Interface running on a PC. (b) Picture of the proposed system.

below 10 mmHg [14]. They are well known for causing mechanical stresses around the brain tissue in chronic implants [15] and because they make difficult to obtain stable intracellular recordings from neurons [16]. Acute extracellular recordings, on the contrary, are less influenced by such micromotions. Neurons with $20-30\ \mu\mathrm{m}$ of diameter or greater, in fact, are estimated to generate a potential of $100\ \mu\mathrm{V}$ or more that can be detected at $100\ \mu\mathrm{m}$ distance if electrodes with electrical impedance of approximately $40-120\ \mathrm{K}\Omega$ are used [17]. For distances larger than $140\ \mu\mathrm{m}$, spikes become indistinguishable from background noise [18]. Although, a moderate pressure applied around the recording site is sufficient to limit the brain pulsation, a real time and reliable control of such pressure is preferable in order to avoid temporary ischemia, which would preclude the possibility to record neural signals. For this reason pressure values should be made available to the surgeon and used in a closed-loop-control system to make the recording device to follow the brain surface at every pressure pulse while keeping the tip of the electrode within $100\ \mu\mathrm{m}$ from the recording site.

A system designed for acute extracellular recordings which fulfils these requirements is presented in this work. It has an autoclavable headstage, an active pressure control system and an electrode inserter. Moreover, here we demonstrate the recording capabilities of our device through several *in-vivo* recording experiments performed on anesthetized rats. The acquired signal quality is comparable to high-quality commercial multichannel systems for laboratory use, while the simplicity of the set-up makes it suitable for a use by medical staff with minimal training.

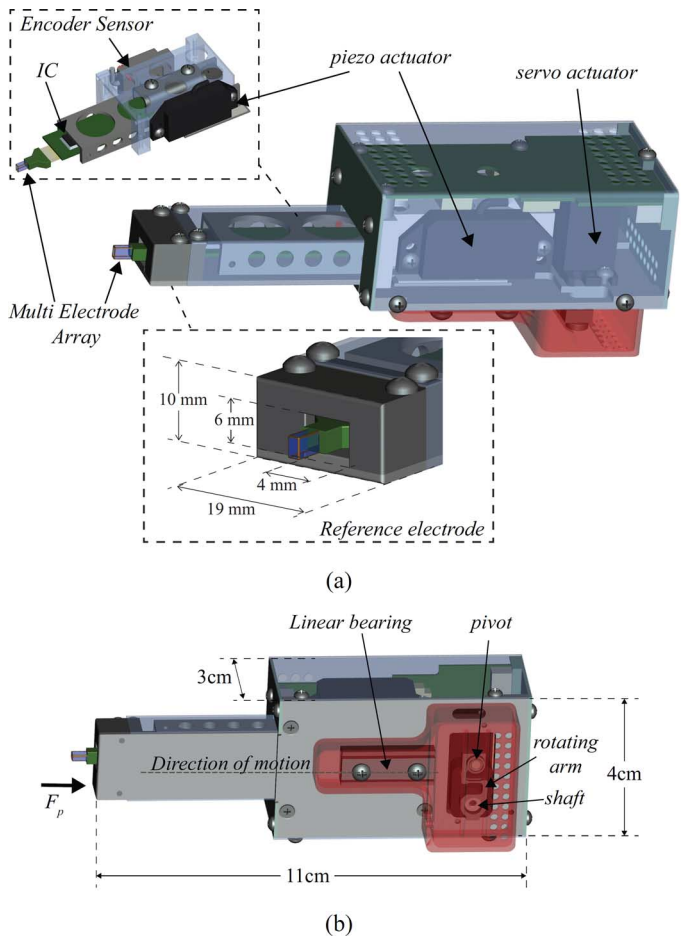

Fig. 2. Detailed view of the headstage. (a) Side view. (b) Bottom view.

II. System Architecture

The neural recording system described in this work is depicted in Fig. 1. It consists of three major parts:

- An autoclavable **headstage** (see Fig. 2) containing:
  - — A neural signal recording module comprising two integrated circuits (IC) with full custom low-noise electronic front-end for single- and multi-unit recordings
  - — An electrode positioning actuator composed of from a stick-slip piezo motor and a position encoder
  - — A headstage positioning actuator with a servo motor
  - — A pressure signal recording module composed of a pressure sensor and a signal amplifier
- A **System Control Unit** (SCU) containing:
  - — A signal processing unit for analog to digital data conversion and signal conditioning
  - — An electrode positioning controller
  - — A headstage positioning controller
- A **Remote User Interface** comprising a Synchronization Unit for precise time stamping of recorded data with respect to external events and a personal computer with a LabView based **Graphical User Interface** (GUI) for real-time visualization of the neural traces, pressure monitoring and for complete control over the whole system.

A. The Headstage Architecture

The headstage represents the most challenging component of the system (see Fig. 2) being a compact and light autoclavable device (size : $11\ \mathrm{cm} \times 4\ \mathrm{cm} \times 3\ \mathrm{cm}$, weight : $\simeq 100\ \mathrm{g}$) which serves as front-end for intra-cortical neural data acquisition. It is set up by the main body, containing the ICs and the motors, and the clamping unit (colored in red in Fig. 2), connected to an articulated arm secured to the border of skull window.

A commercial servo motor controls the position of the headstage on the recording site while a piezo actuator (*P661.P01* , *Physik Instrumente* , *Karlsruhe* , *Germany*) drives the electrodes inside the brain. An optical sensor (*M2000V* , *MicroE systems* , *Bedford—MA* , *USA*) was used for closed loop control of the actual position of the electrodes.

The end tip of the headstage, which defines the contact point with the brain, serves as reference electrode for recording the extracellular signals by two distinct ICs each with eight low-noise and low-power amplifiers. As depicted in Fig. 2(a) it has a small aperture through which the array of electrodes is guided into the brain.

Finally, a pressure sensor is embedded inside the headstage for real time monitoring and control of the pressure exerted by the headstage on the cortical tissue. The signal representing the instantaneous pressure is locally amplified and filtered before being sent to the SCU together with the 16 amplified neural traces.

B. The System Control Unit Architecture

The headstage is connected to the System Control Unit with an unshielded 26-wire ribbon cable. The SCU contains *i)* an Analog Conditioning Board (ACB), *ii)* a Digital Control Unit (DCU) implemented on a Field Programmable Gate Array (FPGA), *iii)* a controller for the piezo actuator (*C867* , *Physik Instrumente* , *Karlsruhe* , *Germany*) and *iv)* the batteries for system power supply.

The Analog Conditioning Board is implemented on a custom Printed Circuit Board (PCB) for analog signal conditioning and Analog to Digital (A/D) conversion of three different input signals: the neural signals recorded by the 16 electrodes, the brain pressure value measured by the sensor and up to 7 additional trigger signals which may be added to provide time synchronization of external events. In this paper we present the system configured to use one external trigger signal.

As depicted in Fig. 3, the 16 amplified neural signals coming from the headstage are band-pass filtered and fed to a Variable Gain Amplifier (VGA) before the A/D conversion. At this stage the user can set via software the high pass cut-off frequency (3 Hz or 300 Hz, for local field potentials of multi-single-unit activity, respectively) of the filter and the additional gain amplification (from $2\times$ to $22\times$) provided by the VGA. The Analog to Digital converter uses 10 bits of resolution and a sampling rate of 40 KHz. Note that, while the neural and the trigger signals are sampled at the maximum sampling rate of 40 KHz, the brain pressure signal was sampled at a lower frequency (i.e., 1 KHz), more than adequate to this kind of signal.

The Digital Control Unit (DCU) implements a set of finite state machines to provide the control signals needed for time

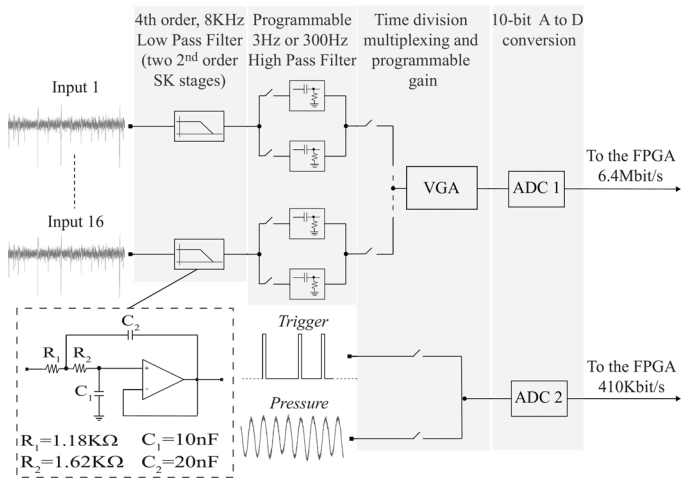

Fig. 3. Conditioning board data path (inset: one of two SK filter stages). The amplified neural traces are further band-pass filtered and amplified before 10-bit A to D conversion. The input trigger and the pressure trace are digitally converted by a dedicated ADC.

division multiplexing of input data as well as for their A/D conversion. Besides, the DCU also implements: *i)* tunable digital filters (both high-pass and low-pass) with programmable order and cut-off frequency for neural signal band-shaping, *ii)* a Universal Serial Bus (USB) interface providing a fast and reliable connection for real-time data read-out and system control, *iii)* a Pulse Width Modulator (PWM) to drive the servo motor which controls the position of the headstage.

Finally, the commercial controller from *Physik Instrumente* is used to manage the closed loop formed by the piezo-actuator and the optic sensor for the precise electrode positioning.

C. The Remote User Interface

The Remote User Interface (RUI) is constituted by a synchronization unit that generates up to 7 synchronization trigger signals, and by a portable personal computer that communicates with the System Control Unit using an USB protocol.

The need of additional trigger signals lies on the fact that functional brain mapping by means of single- and multi-unit recordings requires identification of the brain areas that change their neuronal activity when the patient performs some actions such as speech, hand movements or is presented with sensory stimuli. In these cases, to reach a correct interpretation of acquired data, the experimenter needs to identify precisely when the patient is performing a given task.

The personal computer allows the user to visualize in real time the recorded neural signals and to control the whole system through a Graphical User Interface (GUI) (see Fig. 4) developed in LabVIEW® which can be easily installed as a stand-alone program. The main screen of the GUI is constituted by three panels: one dedicated to the neural data stream, a second one to control the position of the electrodes and a third one to monitor brain pressure and to control headstage position.

The stream of data coming from the FPGA through the USB connection is re-organized in a way that the 16 neural traces and the pressure trace are plotted in two different graphs using a time

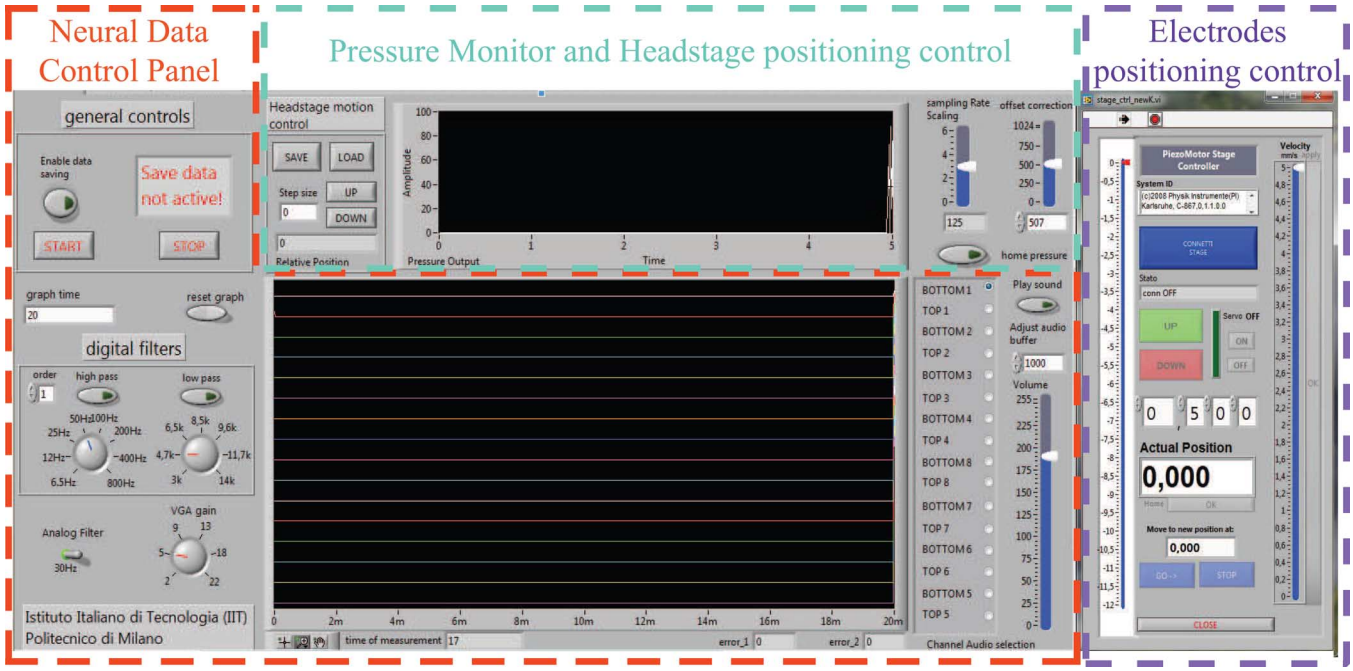

Fig. 4. The Graphical user interface is made up of threee different sections. A panel is dedicated to the neural data stream, a second one to control the position of the electrodes and a third panel to monitor brain pressure and to control headstage position.

window that the user can set and change on-line during acquisition. Several control buttons allow the user to enable/disable the high-pass and low-pass digital filters and to set the values of the cut-off frequencies of the tunable filters. In order to allow the surgeons to distinguish the presence of neuronal activity by listening to the recorded neural signal, the GUI permits the user to select the recorded signal to be sent to the audio output connected to a loudspeaker.

The electrode position control panel on the right side of Fig. 4 has buttons for defining the *home* position, the step size for electrode movement and the velocity at which the electrodes are moved.

III. System Design

In this section we describe in detail the main building blocks of the system.

A. The Headstage Design

Devices designed to be used inside a surgery room must necessarily meet a number of rigorous requirements in order to guarantee the patient's safety. Among them, those that are physically in contact with the patient as the presented headstage, need to be sterilized before each use. Because of its high effectiveness and low cost, the most common method of sterilization is by autoclaving the equipment. However, since the process is unsuitable for heat and humidity sensitive devices, we took special care during headstage design in choosing adequate components and materials. The whole frame, custom designed for reducing size and weight, is made of aluminum, while titanium was preferred for the reference electrode because of its bio-compatibility and being chemically inert. Both motors for headstage and electrode positioning were chosen so that they could withstand the sterilization process.

Finally, signals controlling both the piezo motor and the servo motor are possible sources of noise that can jeopardize the quality of recorded data. For this reason particular care was taken in the layout of the modules inside the headstage and for the routing and shielding of noise sensitive traces carrying analog signals from/to the headstage to/from the system control unit. It is important to notice, however, that electrodes are not moved once the recording site has been reached. Consequently the piezo motor can be turned off during the recording procedure and only noise cross-coupling from the servo motor has to be considered.

A detailed description of the mechanical design and of the sensing units, i.e., the neural amplifiers and the pressure sensor, is provided hereafter.

1) Mechanical Design: The mechanical design of the headstage was critical due to the requirements of being at the same time light, compact and robust, allowing an easy positioning on the recording site and insertion of the electrodes inside the brain.

Two distinct body parts can be distinguished: the main body and the clamping unit. A crank and slide mechanism implemented by the servo motor and the linear bearing [see Fig. 2(b)] permits movements of the clamping unit along the main body by converting the rotary movement of the servo motor into a linear motion along the longitudinal axis. Consequently, since during the recording sessions the clamping unit is fixed to the skull, the described mechanism allows proper placement of the main body on the recording site. Specifically, the headstage is first secured through the clamping unit to the patient's skull and then placed in close vicinity to the recording site with the direction of motion normal to the brain surface as depicted on the left side of Fig. 1(a). At this point the surgeon can remotely reduce the distance from the recording site by using the graphical user interface to control the movement of the main body in order to

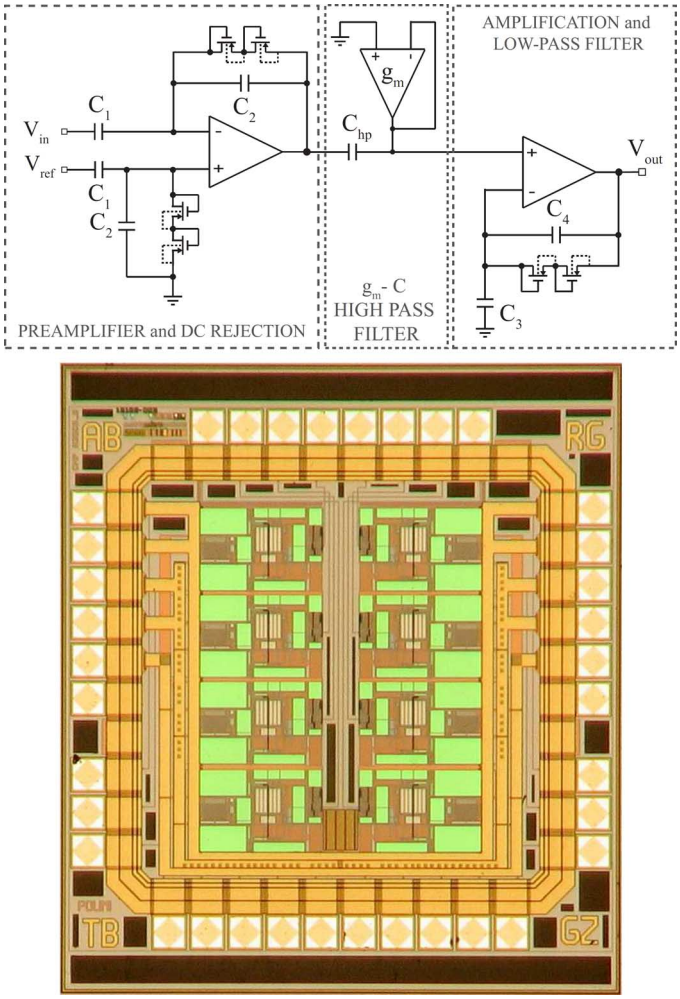

Fig. 5. Three stage low noise neural amplifier implemented in AMS CMOS $0.35\ \mu\mathrm{m}$ technology. (a) Schematic view. (b) Photography of the chip.

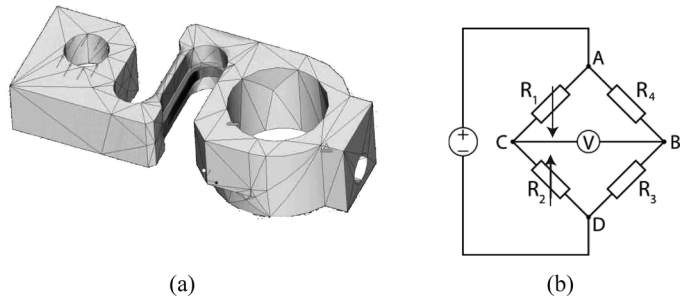

(a) (b)

Fig. 6. A strain gauge based system for pressure monitor is implemented. (a) The stress analysis of the *S* shaped lever arm for a given applied force was used to find the best placement for the strain-gauges: the dark area portrays the largest deformation consequent to an applied force. (b) Wheatstone bridge schematic view.

reach the brain surface. The system has been designed to control the servo motor on the base of the instantaneous pressure in closed loop so as to compensate large brain pulsations.

A sliding aluminum frame placed inside the main body [see insert in Fig. 2(a)] is used for precise insertion of the array of electrodes in the brain. It hosts a small printed circuit board (PCB) with two integrated 8-channel low-noise amplifiers and it is moved by the *stick-slip* piezo actuator while the optical sensor is used for closed loop control of the actual position. The mechanism drives the electrodes inside the brain with a maximum stroke of about 2 cm and a resolution $< 1\ \mu\mathrm{m}$ that is more than adequate to perform intracellular recordings.

2) Integrated Amplifiers: The schematic of the three stage integrated amplifier used to amplify neural signals [19], [20] is depicted in Fig. 5. The first stage is an AC-coupled high-pass filter. The high-pass pole, below 1 Hz, rejects the DC offset and the voltage drift of the electrodes. A high-pass filter is inserted after the first stage to remove the residual offset while a second gain stage provides a further amplification and low-pass filtering. It consists of a single-ended capacitive-coupled voltage amplifier with a low-pass cut-off frequency of about 15 KHz which provides an overall pre-amplifier gain of 58 dB. The power consumption of each pre-amplifier is about $30\ \mu\mathrm{W}$ while the input referred noise is about $3\ \mu\mathrm{V_{rms}}$ in the 10 Hz–15 kHz band and reduces to $2.2\ \mu\mathrm{V_{rms}}$ for the 300 Hz–10 kHz band. The 8-channel integrated circuit was implemented in $0.35\ \mu\mathrm{m}$ austriamicrosystems CMOS technology and packaged in a TQFP48 package.

3) The Pressure Sensor: A strain-gauge based pressure sensor was embedded in the headstage [21] in order to provide the surgeon with the capability to measure and control the pressure exerted on the brain surface during recordings. A linear bearing enables the main body to move along the longitudinal axis with respect to the clamping unit [see Fig. 2(b)]. During a recording session when the closed loop movement control is enabled, the reference electrode is in contact with the brain that pulsates and causes the headstage to move synchronously. Meanwhile the clamping unit is fixed to the skull and, therefore, moves with respect to the headstage. Since the headstage is connected to the clamping unit via a crank and slide mechanism, its movements result in forces exerted on this mechanism.

The small deformation of the lever arm produced by such forces can be measured as the voltage V across a Wheatstone bridge as shown in Fig. 6(b). Here R_1 and R_2 are the equivalent electrical resistance of two properly placed strain gauges which are well known for changing their electrical resistance when stretched or compressed [22]. Because of resistor mismatch, the output voltage V will be affected by an offset which must be compensated in order to avoid output saturation. For this reason, in our implementation, the voltage at point B in the bridge is controlled by means of a Digital to Analog (D/A) converter while the voltage V across the bridge is locally low-pass filtered at 10 Hz before gain amplification and A/D conversion.

Finally, to maximize the sensitivity of the sensor, the lever arm was custom designed, leading to the *S* shape in Fig. 6(a). A stress analysis of the structure was performed in order to find the point of maximum stress for a given applied force, i.e., the best placement for the strain gauges. It is worth noting that the proposed solution keeps the sensor compact and light and, at the same time, improves the sensor sensitivity by a factor of 3 with respect to a straight lever arm.

B. The System Control Unit Design

In order to remove unwanted components before A/D conversion, the recorded neural signals are pass-band filtered with programmable high pass cut-off frequency as depicted in Fig. 3.

The high-pass filter is a first-order RC filter with a user selectable cut-off frequency that can be either set to 3 Hz or 300 Hz; the latter is necessary to remove local field potential (LFP) signals and the line noise interference that is often present in the amplified signal. The low-pass filter, conversely, is a fourth order filter with a cut-off frequency of 8 KHz that was designed by cascading two second order active filters. These latter were implemented using the Sallen-Key (SK) circuit topology depicted inside the dashed black square in Fig. 3 [23], [24]. This filter leaves unmodified the recorded action potentials by reducing the high frequency range and eliminating the alias noise that might occur during the subsequent multiplexing and digitization steps.

After the digitization process, the neural data, the trigger and the pressure signals are fed into the DCU. For safety reasons, a digital isolator is inserted between the A/D converter and the FPGA. In this way the patient is electrically isolated from the personal computer that, when connected to the power line, could be electrically unsafe. This isolation also breaks the current loop through ground wires that may occur between the patient, the headstage, the acquisition system and the personal computer. Moreover, such an electrical isolation reduces the line noise and other electromagnetic interferences. The Digital Control Unit, implemented on an *Opal Kelly* XEM3005–1200M32P integration module based on a 1,200,000-gate Xilinx Spartan-3E FPGA, receives the data stream from the ACU with a rate of 680 KSample/s.

1) Neural Data Processing: a bank of digital filters (high-pass and low-pass) with programmable cut-off frequencies and order is implemented in the DCU, allowing further neural signal band shaping. The pressure trace is digitally low-pass filtered too. Each incoming 10-bit data sample is labeled with a 6-bit header in order to permit a correct data reconstruction during the read out on the PC (see Fig. 7). The resultant encoded data are temporarily stored and periodically read via USB connection without any data loss. Both raw and digitally filtered data are sent to the personal computer: raw data are saved in separated files (one for each channel) while the digitally filtered data are plotted on the graphical user interface.

2) Headstage Position Control: a pulse width modulator (PWM) is implemented on the FPGA for complete and precise control of the servo motor for the headstage positioning ($50\ \mu\mathrm{m}$ resolution), and can be driven either in open or closed loop mode. When the open loop mode is selected, the servo motor position is set by the user through the graphical interface. On the contrary, in closed loop mode, the servo motor position is automatically adjusted in order to compensate any change of pressure between the device and the brain.

For this purpose we implemented a proportional-integral-derivative (PID) closed-loop control on the FPGA. Given the controlled pressure and its desired value, named P and P_d respectively, the goal is to eliminate the error between P and P_d. The value of P is measured by the sensor and is compared

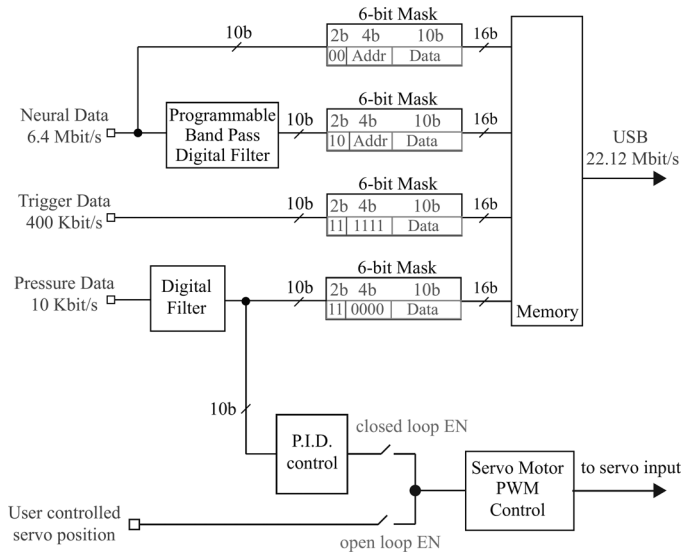

Fig. 7. Digital data path: incoming digital data are properly labeled before being sent to a PC via USB cable. The servo motor for headstage positioning can be controlled in either open loop or closed loop mode.

with P_d to produce the error $e(t)$. The output $u(t)$ from the closed-loop controller can be described by a differential equation that, for a small sample interval, can be discretized as in 1 to implement the so called "incremental algorithm " [25].

$$u(n) = u(n-1) + K_0 e(n) + K_1 e(n-1) + K_2 e(n-2) \quad (1)$$

Since 1 is characterized by the calculation of the control output, $u(n)$, based on $u(n-1)$ and the correction term $\Delta u(n) = u(n) - u(n-1)$, accumulation of all past errors $e(n)$ is avoided with a significant saving of FPGA resources. Coefficients K_i are finally derived by the proportional, integral and derivative gains ($K_0 = K_p + K_i + K_d$, $K_1 = -K_p - 2K_d$ and $K_2 = K_d$).

Since the PID algorithm is implemented on the FPGA (whose clock frequency is of about 30 MHz) the maximum available bandwidth of the closed-loop-control is set by the servo motor. This, as derived by motor specifications, has a maximum speed of 1 cm/140 ms, meaning that in the worst case scenario the system permits to follow oscillations as large as 1 cm, provided that these are slower than 7 Hz (1/140 ms). This bandwidth is more than adequate to permit the system to follow the micro-motions of the brain, which are expected to have amplitudes of about $0.5\ \mathrm{mm}$ and frequency below 2 Hz.

IV. Results

A. Recording Capabilities

The recording capabilities of our system were tested on anestethized animals. Experiments were carried out in acute sessions on Long-Evans male rats, weighing 300–400 g anaesthetized with a mixture of Zoletil (30 mg/Kg) and Xylazine (5 mg/Kg) delivered intraperitoneally. The animals were placed in a stereotaxic instrument and a small craniotomy (2 mm×2 mm) was made in the parietal bone. The primary

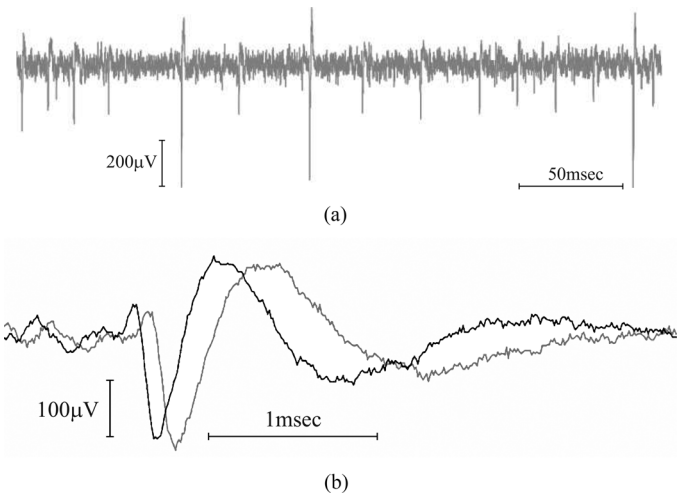

Fig. 8. Neural traces recorded from a rat cortex. (a) Sample of recording. (b) Direct comparison of data recorded with our and Plexon system. Tests showed that even weak single units ($\simeq$ 30 μV_{pp}) can be detected and the parallel recording with a Plexon commercial system shows minimal differences between the signals acquired with our system (dark grey) and with the MAP commercial set up (pale gray).

somatosensory cortex was exposed and dura mater was left intact. The electrodes were lowered perpendicular to the cortical surface to a depth of about 700 μm.

We tested the operation of the trigger signal by mechanically stimulating the rat whiskers by a mini-shaker, inducing in this way evoked neural activity in the somatosensory cortex. The whiskers stimulation consisted of 30 trains, each one made by 10 pulses, delivered at 10 Hz, with a pause of 5 seconds between each train [26]. In this case the trigger signal was a square wave indicating the occurrences of each pulse.

Before the recording sessions, both the headstage and the connection cable with the System Control Unit underwent a number of sterilization cycles in autoclave. Autoclaving parameters were set in accordance with the procedure followed for sterilization of surgical instruments (30 minutes, 120°C and 100% humidity). Both motors for electrode and headstage positioning as well as the recording capabilities and the pressure sensor were extensively tested after each cycle. The overall performances of the headstage remained unaffected although during our tests it underwent tens of sterilization processes.

The noise injected by the servo motor on the recording data path was also evaluated. We immersed the tip of the electrodes in a 0.9% saline solution. A 1 KHz pure sine wave with 100 μV of amplitude was injected and data were acquired with the servo motor turned ON and OFF. Fig. 10 shows the FFT output in both cases. Notice that the noise floor is slightly below when the servo motor is OFF, passing from 2.9 μV_{rms} to 3.1 μV_{rms} when it is turned ON.

Direct comparison with a commercial recording system (*Multichannel Acquisition Processor (MAP)*, *Plexon Inc*, *Dallas*, *USA*) showed that the noise levels and distortions introduced by our amplifier chain are minimal [Fig. 8(b)]. Specifically, in the signal band of 0.3 – 7 KHz , the noise levels are almost identical for the two systems. For instance, in the recorded signals shown in Fig. 8(a), the noise level of

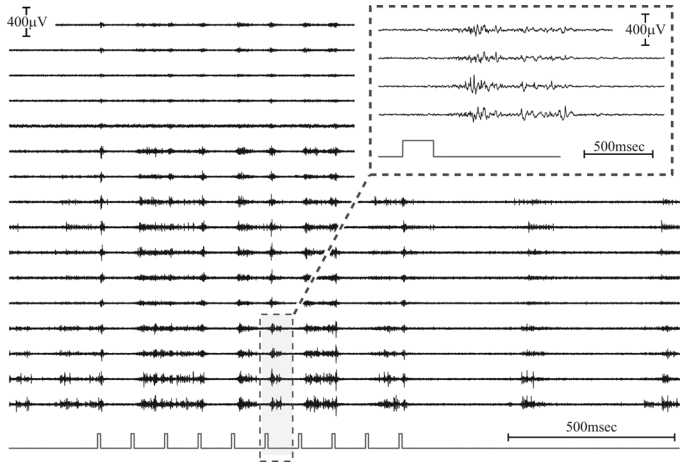

Fig. 9. 16 neural traces recorded from a rat cortex during mechanical stimulation of the rat's whiskers and (bottom trace) the trigger signal indicating the occurrences of each stimulus. In the insert the evoked neural responses from 4 channels upon a mechanical stimulus are shown.

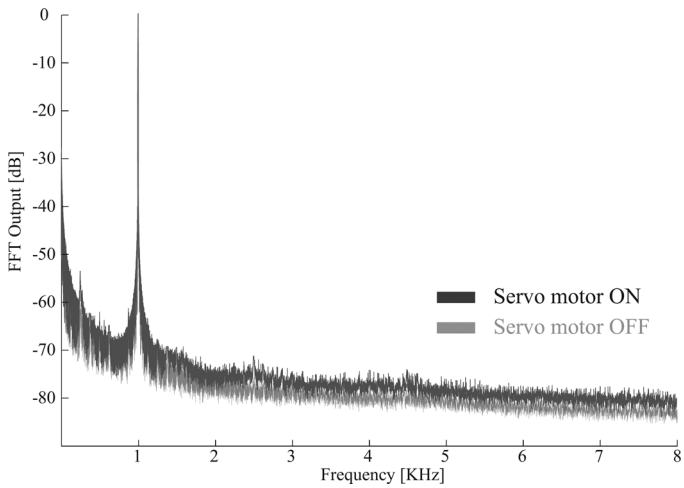

Fig. 10. Evaluation of the noise injected by the servo motor on the recorded data. FFT outputs for the same 1 KHz, 100 μV pure sine wave acquired with the servo motor turned ON and OFF.

our trace was 8.3 μV_{rms} while it was 8.9 μV_{rms} for the trace obtained with the Plexon MAP. The bench-top tests showed that the noise of the whole system including all connections was below 3 μV_{rms} in the 0.3 – 7 KHz band that is similar to the specifications of the MAP system (below 5 μV_{rms} according to the datasheet or $\sim$ 3 μV_{rms} according to our measurements). Fig. 9 shows the neural signals acquired from each electrode of the array.

B. Pressure Compensation Performances

The pressure sensor and the related closed loop position control were tested under controlled conditions. To evaluate the static performances, we applied loads of up to 200 g with minimum steps of 2 g. This dynamic range value has been chosen taking into account the fact that the system, while operating in closed loop, must be able to move the whole headstage to compensate any change of the measured instantaneous pressure.

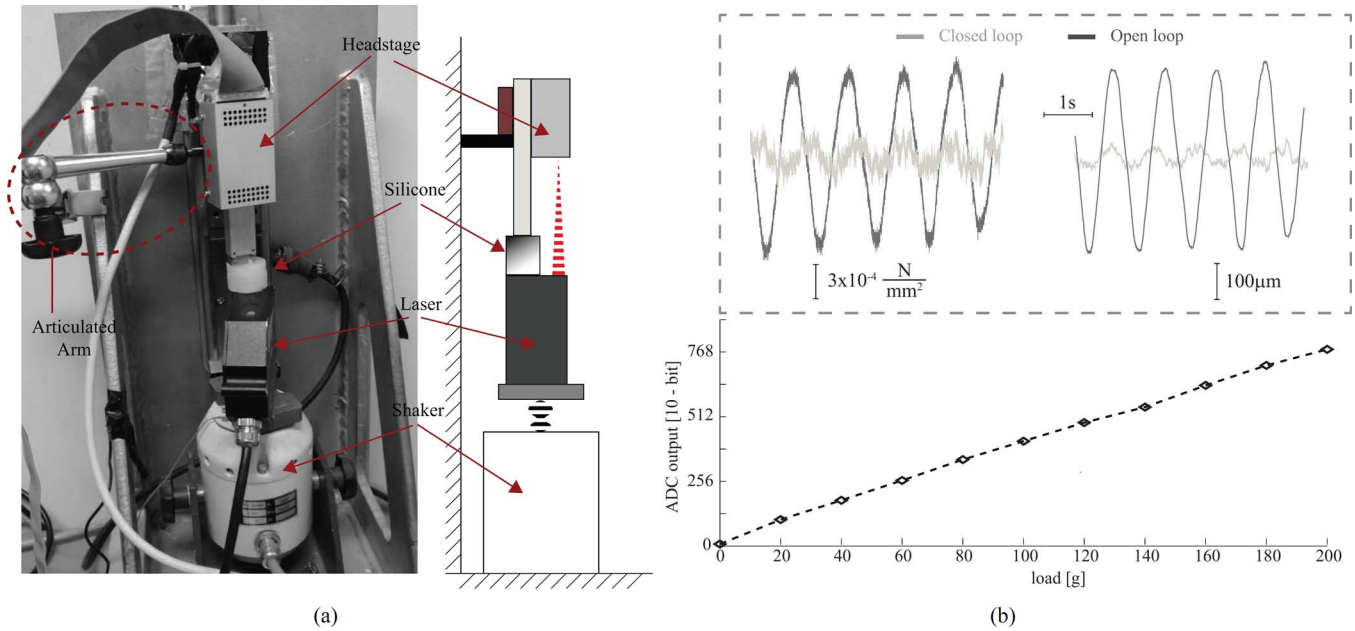

(a) (b)

Fig. 11. (a) Experimental setup used to evaluate the dynamic performances of the pressure sensor: picture (left side) and schematic view (right side). (b) Bench test results for the strain gauge based pressure sensor. The static characteristic shows a good linearity in the 0-200 g range (bottom). The dynamic performance for an applied 1 Hz force stimuli shows how in closed loop mode the measured pressure is significantly reduced (top left) while the resultant displacement is less then 100 μm (top right).

Since the weight of the headstage is of about 100 g, a smaller dynamic range would lead to output saturation and hence to the inability of controlling the headstage position in accordance with the measured pressure. The dynamic performances were tested by means of the experimental setup shown in the left side of Fig. 11(a) (the schematic representation is depicted on the right side). The headstage was anchored through the clamping unit to a frame rigidly coupled to the workbench using an articulated arm that is commonly used in the surgery room. A voltage controlled shaker (TIRA, Model—TV50018) was finally used to apply dynamic vertical forces. In order to match the test bench as close as possible to the physiology, the oscillations were designed to produce pressure variations that are comparable with typical pressure measurements taken from clinical cases [14]. The mechanical properties of the brain were finally emulated by using a sample of soft silicone pad whose Young's modulus was comparable with the one reported in [27] for the human brain. The pad was placed between the reference electrode of the headstage and a laser triangulation sensor from Micro-Epsilon (optoNCDT 2300, *Micro-Epsilon Messtechnik GmbH & Co.*, KG, *Germany*), this latter positioned on the top of the shaker as depicted on the right side of Fig. 11(a). By this way, for any force applied by the shaker, we were able to measure both the instantaneous pressure sensed by our integrated sensor (with a resolution of about 1 $\mu\mathrm{N}/\mathrm{mm}^2$) as well as the distance of the main body of the headstage from the laser and, consequently, the resulting compression of the silicone pad (with a 1 μm resolution).

The system was tested by applying oscillating input signals with maximum amplitude and frequency respectively set to 2 mm and 4 Hz, both four times larger than what expected from actual brain pulsations. The results of these tests are shown in Fig. 11(b). More in detail, on the bottom side is shown the good linearity of the input-output characteristic of the sensor resulting from the static measurements while on the top side are reported the results of the dynamic tests for an applied 1 Hz sinusoidal force stimuli with a 600 μm amplitude. The closed loop control of the servo motor reduces by severalfold both the measured pressure (top-left side) and the compression of the silicone, the latter decreasing from around ± 300 μm to ± 50 μm. As already stated, electrodes with electrical impedance of approximately $40 - 120$ kΩ, as those expected to be used with our system [28], are estimated to record from a sphere with a radius of 100 μm [17]. Consequently our results show that the proposed system is not only able to compensate pressure variations but it is also potentially capable of keeping the electrodes within a volume of brain tissue small enough to keep stable acute extracellular recording quality (particularly for LFP).

V. Conclusions

In this paper we describe a multichannel single- and multi-unit recording system with a software-controlled manipulator that can be used for intra-operative brain monitoring during functional detections along and inside the tumor in human patients. With its two motors for precise headstage positioning and electrode insertion, the integrated low-noise and low-power amplifiers for neural signal amplification and the embedded sensor pressure, the headstage is certainly the most challenging component of the presented system. Thanks to a proper choice of components and materials for its realization, the performances of the system are unaffected by an autoclave sterilization with a standard cycle of 120°C and 100% humidity.

The choice of exploiting the contact point as reference electrode had a positive consequence. The large area of the reference electrode (more than 5 times the size of the whole micro-wire array) resulted in a finer differentiation among signals coming

from the 16 micro-wires. At the same time, this large contact point provides a mean to locally reduce brain pulsation during recordings while the embedded sensor allows real time monitoring and controlling over the pressure exerted on the recording site.

Concluding, although a number of multichannel systems are already commercially available, the vast majority of them are relatively bulky and expensive. Most importantly, none of them allows real-time measure and control of the pressure exerted on the brain during recordings. Our system is very compact (one small rack box and a portable computer), has no expensive elements and is very reliable and simple to use. For these reasons, we believe that it may represent an important step towards the development of new certified systems to be used into a surgery room for intra-operative brain mapping.

Acknowledgment

The authors would like to thank A. Mazzoni for the useful help with neural data analysis, D. Torazza for the mechanical design, and L. Taverna for graphic elaborations.

References

[1] B. Guthrie and E. Laws, "Supratentorial low-grade gliomas," *Neurosurgery Clin. North Amer.*, vol. 1, pp. 37–48, 1990.

[2] F. Pignatti *et al.*, "Prognostic factors for survival in adult patients with cerebral low-grade glioma," *J. Clin. Oncology*, vol. 20, no. 8, pp. 2076–2084, 2002.

[3] M. Berger and N. Sanai, "Glioma extent of resection and its impact on patient outcome," *Neurosurgery*, vol. 62, pp. 753–766, 2008.

[4] J. Smith, E. Chang, K. Lamborn, S. Chang, M. Prados, S. Cha, T. Tihan, S. VandenBerg, M. McDermott, and M. Berger, "Role of extent of resection in the long-term outcome of low-grade hemispheric gliomas," *J. Clin. Oncology*, vol. 26, no. 8, pp. 1338–1345, 2008.

[5] T. Ius, M. Isola, R. Budai, G. Pauletto, B. Tomasino, L. Fadiga, and M. Skrap, "Low-grade glioma surgery in eloquent areas: volumetric analysis of extent of resection and its impact on overall survival. A single-institution experience in 190 patients," *J. Neurosurgery*, vol. 117, no. 6, pp. 1039–1052, 2012.

[6] H. Duffau *et al.*, "Usefulness of intraoperative electrical subcortical mapping during surgery for low-grade gliomas located within eloquent brain regions: functional results in a consecutive series of 103 patients," *J. Neurosurgery*, vol. 98, no. 4, pp. 764–778, 2003.

[7] G. Neuloh, U. Pechstein, C. Cedzich, and J. Schramm, "Motor evoked potential monitoring with supratentorial surgery," *Neurosurgery*, vol. 54, no. 5, pp. 1061–1072, 2004.

[8] M. Berger, S. Ghatan, M. Haglund, J. Dobbins, and G. Ojemann, "Low-grade gliomas associated with intractable epilepsy: seizure outcome utilizing electrocorticography during tumor resection," *J. Neurosurgery*, vol. 79, no. 1, pp. 62–69, 1993.

[9] M. Berger and R. Rostomily, "Low grade gliomas: functional mapping resection strategies, extent of resection, and outcome," *J. f Neuro-Oncology*, vol. 34, no. 1, pp. 85–101, 1997.

[10] V. Majidzadeh, A. Schmid, and Y. Leblebici, "Energy efficient low-noise neural recording amplifier with enhanced noise efficiency factor," *IEEE Trans. Biomed. Circuits Syst.*, vol. 5, no. 3, pp. 262–271, Jun. 2011.

[11] W. Wattanapanitch and R. Sarpeshkar, "A low-power 32-channel digitally programmable neural recording integrated circuit," *IEEE Trans. Biomed. Circuits Syst.*, vol. 5, no. 6, pp. 592–602, Dec. 2011.

[12] C. M. Lopez, D. Prodanov, D. Braeken, I. Gligorijevic, W. Eberle, C. Bartic, R. Puers, and G. Gielen, "A multichannel integrated circuit for electrical recording of neural activity, with independent channel programmability," *IEEE Trans. Biomed. Circuits Syst.*, vol. 6, no. 2, pp. 101–110, Dec. 2012.

[13] E. Pralong, J.-G. Villemure, J. Bloch, C. Pollo, R. T. Daniels, J. Ghika, F. Vingerhoets, M. H. Tetreault, and D. Debatisse, "Quality index for the quantification of the information recorded along standard microelectrode tracks to the subthalamic nucleus in parkinsonian patients," *Neurophysiol. Clin.*, vol. 34, no. 5, pp. 209–215, 2004.

[14] M. E. Wagshul, P. K. Eide, and J. R. Madsen, "The pulsating brain: a review of experimental and clinical studies of intracranial pulsatility," *Fluids Barriers CNS*, vol. 8, no. 1, p. 5, 2011.

[15] A. Gilletti and J. Muthuswamy, "Brain micromotion around implants in the rodent somatosensory cortex," *J. Neural Eng.*, vol. 3, no. 3, p. 189, 2006.

[16] R. Britt and G. Rossi, "Quantitative analysis of methods for reducing physiological brain pulsations," *J. Neurosci. Methods*, vol. 6, no. 3, pp. 219–229, 1982.

[17] W. Rall, "Electrophysiology of a dendritic neuron model," *Biophysi. J.*, vol. 2, no. 2, pt. 2, p. 145, 1962.

[18] D. A. Henze, Z. Borhegyi, J. Csicsvari, A. Mamiya, K. D. Harris, and G. Buzsáki, "Intracellular features predicted by extracellular recordings in the hippocampus in vivo," *J. Neurophys.*, vol. 84, no. 1, pp. 390–400, 2000.

[19] A. Bonfanti, T. Borghi, R. Gusmeroli, G. Zambra, A. Oliyink, L. Fadiga, A. Spinelli, and G. Baranauskas, "A low-power integrated circuit for analog spike detection and sorting in neural prosthesis systems," in *Proc. IEEE Biomedical Circuits and Syst. Conf.,* , 2008, pp. 257–260.

[20] A. Bonfanti, M. Ceravolo, G. Zambra, R. Gusmeroli, A. Spinelli, A. Lacaita, G. Angotzi, G. Baranauskas, and L. Fadiga, "A multi-channel low-power system-on-chip for single-unit recording and narrowband wireless transmission of neural signal," in *Proc. Annu. Int. Conf. IEEE Eng. Medicine and Biology Soc.*, 2010, pp. 1555–1560.

[21] G. N. Angotzi, L. Fadiga, and G. Sandini, A dynamic brain pressure control for single unit in vivo neural recordings, Patent O2011A000516, PCT/IB2012/052 948.

[22] G. Witt, "The electromechanical properties of thin films and the thin film strain gauge," *Thin Solid Films*, vol. 22, no. 2, pp. 133–156, 1974.

[23] R. Sallen and E. Key, "A practical method of designing RC active filters," MIT Lincoln Laboratoyr, 1954.

[24] B. Razavi*, Fundamentals of Microelectronics*. Hoboken, NJ, USA: Wiley, 2009, vol. 1.

[25] R. Isermann*, Digital Control Systems*. New York, NY, USA: Springer-Verlag, 1991, vol. 2, Stochastic Control, Multivariable Control, Adaptive Control, Applications.

[26] A. Lak, E. Arabzadeh, J. A. Harris, and M. E. Diamond, "Correlated physiological and perceptual effects of noise in a tactile stimulus," *Proc. Nat. Acad. Sci.*, vol. 107, no. 17, pp. 7981–7986, 2010.

[27] H. Metz, J. McElhaney, and A. K. Ommaya, "A comparison of the elasticity of live, dead, and fixed brain tissue," *J. Biomech.*, vol. 3, no. 4, pp. 453–458, 1970.

[28] Trucker-davis technoligies microwire arrays [Online]. Available: http://www.tdt.com/products/MW16.htm#OMN1010